Supporting information

How metal/support improved degradation performance in peroxymonosulfate activation process: Significance of high-valent cobalt-oxo species

Xing Fan,[1abc] Wei Zhang,[1abc] Huchuan Yan,[abc] Cui Lai,[*abc] Dengsheng Ma,[ab] Shiyu Liu,[abc] Mingming Zhang,[abc] Ling Li,[abc] Xuerong Zhou,[abc] Xiuqin Huo,[abc] Fuhang Xu,[abc] Xiaorui Hu,[ab] Biting Wang,[ab] Hao Sun[ab], Wuqiang He[d]

[a] College of Environmental Science and Engineering, Hunan University, Changsha 410082, PR China,

[b] Key Laboratory of Environmental Biology and Pollution Control, Hunan University, Ministry of Education, Changsha 410082, PR China,

[c] Research Institute of Hunan University In Chongqing, Chongqing 401120, PR China,

[d] College of Materials and Advanced Manufacturing, Hunan University of Technology, Zhuzhou 412007, China.

∗ Corresponding author at: College of Environmental Science and Engineering, Hunan University, Changsha, Hunan 410082, China. Tel: +86–731–88822754; fax: +86–731–88823701. E-mail address: laicui@hnu.edu.cn (C.Lai).

1 These authors contribute equally to this article.

Contents

Fig. S4. Effect of PMS dosage (a) and catalyst dosage (b) on 10-CFS/PMS system.

Fig. S5. Time-dependent UV-vis absorption spectrum changes of DPBF consumption in the physical mixing system of $CoFe_2O_4$ and sepiolite (a), 10-CFS/PMS (b) activation system, and 10-CFS/PMS activation system with the addition of TEMPO before PMS activation (c). Reaction conditions: [CIP] = 10 mg/L, [10-CFS] = 0.1 g/L, [PMS] = 0.5 mM, [DPBF] =0.15 mM.

Fig. S6. CIP degradation in the 10-CFS/PMS system with or without Ar bubbling. Reaction conditions: [CIP] = 10 mg/L, [10-CFS] =0.1 g/L, [PMS] = 0.5 mM.

Fig. S7. EPR spectra for $^1O_2$ (a), $O_2^{\cdot-}$ (b), and $SO_4^{\cdot-}$and $HO^{\cdot}$ (c) in the 10-CFS/PMS system.

Fig. S8. Degradation efficiency of CIP, NB, and BA in the 10-CFS/PMS system. Reaction conditions: [CIP] = 10 mg/L, [NB/BA] =0.008 mM, [10-CFS] = 0.1 g/L, [PMS] = 0.5 mM.

Fig. S9. Concentration variation of PMSO and $PMSO_2$ in the 10-CFS/PMS system. Reaction conditions: [PMSO]=0.1 mM, [10-CFS] = 0.1 g/L, [PMS] = 0.5 mM.

Fig. S10. In situ Raman spectra of 10-CFS/PMS system in H_2O matrix.

Fig. S11. The model of 10-CFS (a) and $CoFe_2O_4$ (b). The O, Mg, Si, Co and Fe atoms are represented by red, orange, blue, pink and brown spheres, respectively.

Fig. S12. XPS spectra of Co 2p (a), Fe 2p (b), O 1s (c) and Si 2p (d) of 10-CFS before and after the reaction.

Fig. S13. The quenching experiments to prove Co and Fe active sites. Reaction conditions: [CIP] = 10 mg/L, [10-CFS] = 0.1 g/L, [PMS] = 0.5 mM, [NaF] = 2 mM.

Fig. S14. Reusability of 10-CFS. Reaction conditions: [CIP] = 10 mg/L, [10-CFS] = 0.1 g/L, [PMS] = 0.5 mM.

Fig. S15. XRD of fresh and used 10-CFS.

Totally 32 pages containing 7 Texts, 3 Tables and 15 Figures.

Text S1. Chemicals and materials

Sepiolite, ciprofloxacin (CIP), tetracycline (TC), methyl phenyl sulfoxide (PMSO) and methyl phenyl sulphone ($PMSO_2$) were purchased from Shanghai Rhawn Chemical Regent Co., Ltd. Cobalt nitrate ($Co(NO_3)_2·6H_2O$), ferric nitrate ($Fe(NO_3)_3·9H_2O$), sodium hydroxide (NaOH), methanol (MeOH), tert-butyl alcohol (TBA), sodium chloride (NaCl), sodium nitrate ($NaNO_3$), sodium sulfate (Na_2SO_4), sodium dihydrogen phosphate (NaH_2PO_4), benzoic acid (BA) and nitrobenzene (NB) were purchased by Sinopharm Chemical Actual Co. Peroxymonosulfate ($KHSO_5·0.5KHSO_4·0.5K_2SO_4$, PMS) was purchased from Shanghai Aladdin Biochemical Technology Co., Ltd. 4-chlorophenol (4-CP) was purchased from Shanghai Maclin Biochemical Technology Co., Ltd. Sulfamethoxazole (SMX) was bought from Xianding Biological Technology Co., Ltd. (Shanghai, China). All experiment process used ultrapure water (18.25 MΩ) to prepare solutions.

Text S2. CIP degradation experiments

Specifically, the catalyst (10 mg) was dispersed into 100 mL of target pollutant solution and stirred magnetically for 30 min to achieve the adsorption/desorption equilibrium. Then, quantified PMS (0.5 mM) was added to the above mixture solution to start the catalytic oxidation. After a certain interval, a 1.5 mL sample solution was taken, filtered with 0.22 μm filter, and then transferred into a vial containing 20 μL sodium thiosulfate solution (0.5 M) to quench the PMS activation reactions. All experiments were conducted in duplicates at least, and the mean values with standard deviations were reported.

Text S3. Determination of PMS concentrations

Residual PMS was quantified. Specifically, 0.2 mL sample was added into 2.8 mL of KI (214.29 g/L)/$NaHCO_3$ (42.86 g/L) solution. Then the mixed solution was shaken for 20 minutes to ensure a complete reaction. Finally, it was determined by a UV-Vis spectrophotometer at the wavelength of 352 nm.

Text S4. Characterization methods

The X-ray diffraction (XRD, Bruker D8 Advance X-ray diffractometer) was adopted to identify the crystallography of the catalysts. The morphological characteristics were observed by scanning electron microscope (SEM, Zeiss Sigma 300), transmission electron microscopy (TEM, jem2100), and high-resolution TEM (HR-TEM). The Fourier transform infrared spectroscopy (FTIR, Thermo Scientific Nicolet iS20) was used to determine functional groups. The chemical states of various elements of catalysts were investigated by X-ray photoelectron spectroscopy (XPS, Thermo Scientific K-Alpha). The electron paramagnetic resonance (EPR) measurement was carried out on a Bruker EMX PLUS spectrometer to detect the reactive oxygen species, in which 5,5-dimethyl-1-pyrroline N-oxide (DMPO) and 2,2,6,6-tetramethylpiperidinyloxyl (TEMP) were applied as the spin-trap reagent. In-situ Raman spectra was acquired under a HORIBA HR Evolution dispersive Raman microscope at λ=532 nm. In addition, the concentration of DPBF was measured by UV-2700 spectrophotometer (Shimadzu Corporation) at 411 nm.

Text S5. DFT Computational methods

First-principal calculations were conducted using density functional theory (DFT) with the Vienna ab-initio simulation package (VASP).[1] The generalized gradient approximation (GGA) with the Perdew−Burke−Ernzerhof (PBE) functional was used to describe the electronic exchange and correlation effects.[2] Atomic positions were relaxed until the forces were less than 0.04 eV/Å. The energy cutoff of the plane wave was set to 400 eV. The criteria for the relaxation of the electronic SC-loop was set to be 1×10^{-6} eV $Å^{-1}$.The Brillouin zone was sampled using a Gamma k-point of 1 × 1 × 1. The pre- and post-processing of the calculation were finished via the VASPKIT.[3] The calculation results are presented by VESTA.[4] In order to accurately investigate the effect of the d orbitals of Fe and Co on the electronic properties of the catalysts, the Hubbard parameter is introduced for the Fe 3d and Co 3d electrons with an U_{eff} (=U−J) value of 3.2 eV and 3.32 eV, respectiely. The van der Waals interactions were considered based on zero damping DFT-D3 method of Grimme.[5] A modified PBE generalization (PBEsol) was used to model the adsorption of PMS on the catalyst surface. The energy of the adsorption system is finally corrected under the PBE function. The model for $CoFe_2O_4$ and sepiolite was derived from the materials-project.[6] The adsorption energy E_{ads} of PMS was noted below:

$$E_{ads} = E_{slab + PMS} - E_{slab} - E_{PMS}$$

where $E_{slab+PMS}$ represents the total energy of the system formed by an adsorbed PMS and the slab, E_{slab} is the energy of the slab, E_{PMS} refers to the energy of the isolated PMS. The change in Gibbs free energy at each step was calculated based on the

following equation:

$$\Delta G = \Delta E + \Delta ZPE - T\Delta S$$

where ΔE belongs to the reaction energy obtained by the total energy difference between the reactant and product molecules absorbed on the catalyst surface, ΔZPE represents the correction of zero-point energy, T refers to the temperature (298.15 K) and ΔS is the entropy change.

Text S6. EPR analyses

EPR tests were employed to distinguish the reactive oxygen species (ROS) in the 10-CFS/PMS system. In Fig. S7b, the characteristic signal of DMPO-$O_2^{\cdot-}$ emerged. In Fig. S7a, the typical signal of TEMP-$^1O_2$ (1:1:1) is detected in the 10-CFS/PMS system. And it is worth mentioning that the intensity of the signal enhances with reaction time, which indicates that $^1O_2$ be continuously produced during the PMS activation process.

Text S7. The competition kinetics experiment in the mixed solution containing NB, BA, and CIP.

To evaluate the contribution of different reactive species to CIP degradation in the 10-CFS/PMS and physical mixed 10-CFS/PMS systems, the competition kinetics experiment in the mixed solution containing NB, BA, and CIP was carried out.[7] It is worth noting that the oxidation removals of three pollutants was gained by deducting the adsorption contribution. According to the reported second-order rate constants of $SO_4^{\cdot-}$ and $HO^{\cdot}$ with the three probe compounds (Table S3) along with the experiment results (Fig. 3e), the steady-state concentration and the relative contribution of $HO^{\cdot}$ and $SO_4^{\cdot-}$ are obtained based on Eqs. 1-6, respectively.

Table S1. The HPLC analysis conditions for different substrates.

Substrates	Flow (ml/min)	λ (nm)	CH_3OH (%)	H_2O (%)	CH_3CN (%)	0.1% HCOOH (%)
CIP	1.0	278	—	—	20	80
BA	1.0	230	70	—	—	30
NB	1.0	262	—	—	50	50
4-CP	1.0	280	70	30	—	—
SMX	1.0	264	—	—	30	70
PMSO	1.0	230	—	80	20	—
$PMSO_2$	1.0	215	—	80	20	—

Table S2. Comparison of PMS activation performance of 10-CFS with other reported catalysts

Catalyst (g/L)	PMS (mM)	Pollutant (mg/L)	Removal efficiency	k_{obs} (min^{-1})	Ref
10-CFS (0.1)	0.5	Ciprofloxacin (10)	98.7% (60 min)	0.127	This work
MNBC (0.8)	0.7	Ciprofloxacin (10)	92.6% (80 min)	0.020	[8]
$CoFe_2O_4$/OSC (0.5)	0.8	Norfloxacin (10)	90.8% (60 min)	0.051	[9]
$CoFe_2O_4$/mpg-C_3N_4 (0.04)	1.5	Acetaminophen (15)	92.0% (25 min)	0.102	[10]
$CoFe_2O_4$/Al_2O_3 (0.2)	0.5	Sulfachloropyridazine (5)	97.8% (60 min)	0.044	[11]
MBC/ $CoFe_2O_4$ (0.6)	0.7	Lomefloxacin hydrochloride (10)	86.9% (20 min)	0.043	[12]

Table S3. Second order rate constants (M^{-1} s^{-1}) of radicals toward probe compounds

Probe	$HO^{\cdot}$	$SO_4^{\cdot -}$
Nitrobenzene (NB)	4.70×10^{9}[a]	—
Benzoic acid (BA)	2.10×10^{9}[a]	1.20×10^{9}[a]
Ciprofloxacin (CIP)	2.35×10^{9}[b]	2.10×10^{9}[b]

Note: a,[7] b[13]

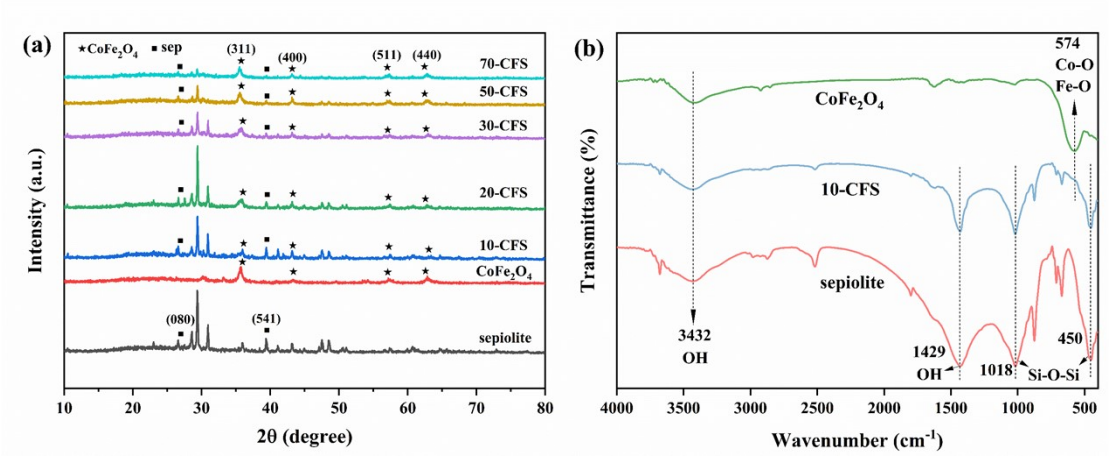

Fig. S1. XRD patterns (a), FTIR spectra (b) of different catalysts.

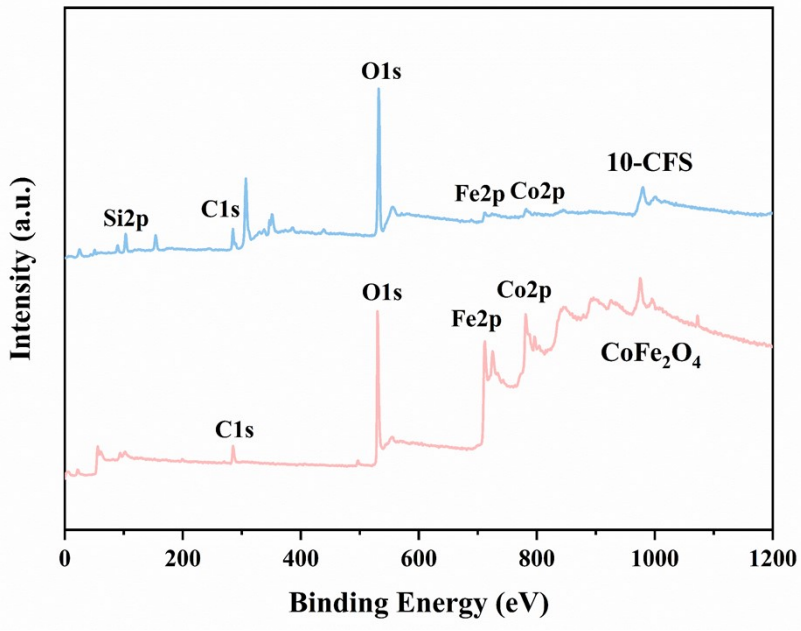

Fig. S2. The XPS spectra of $CoFe_2O_4$ and 10-CFS survey.

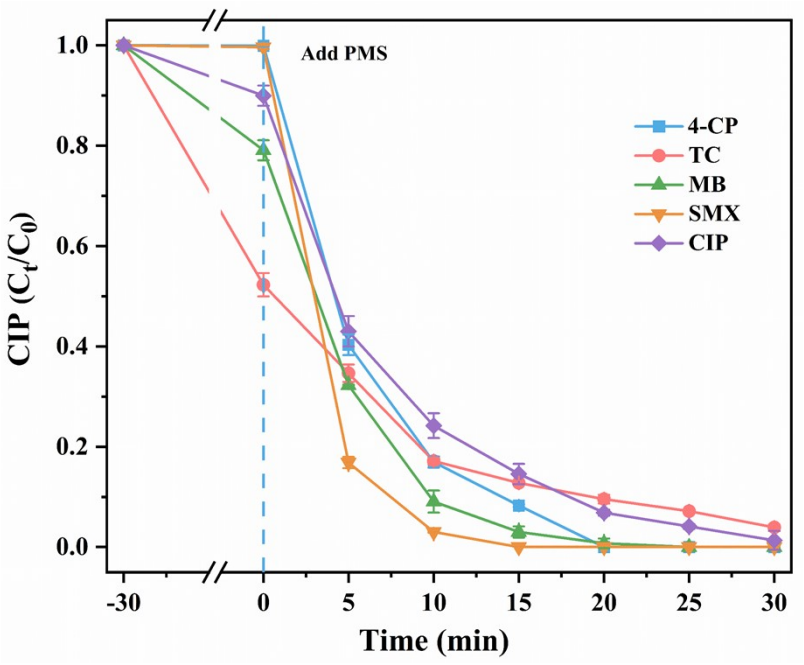

Fig. S3. Removal efficiency of various contaminants in the 10-CFS/PMS system. Reaction conditions: $[pollutant]_0$= 10 mg/L, [10-CFS] = 0.1 g/L, [PMS] = 0.5 mM.

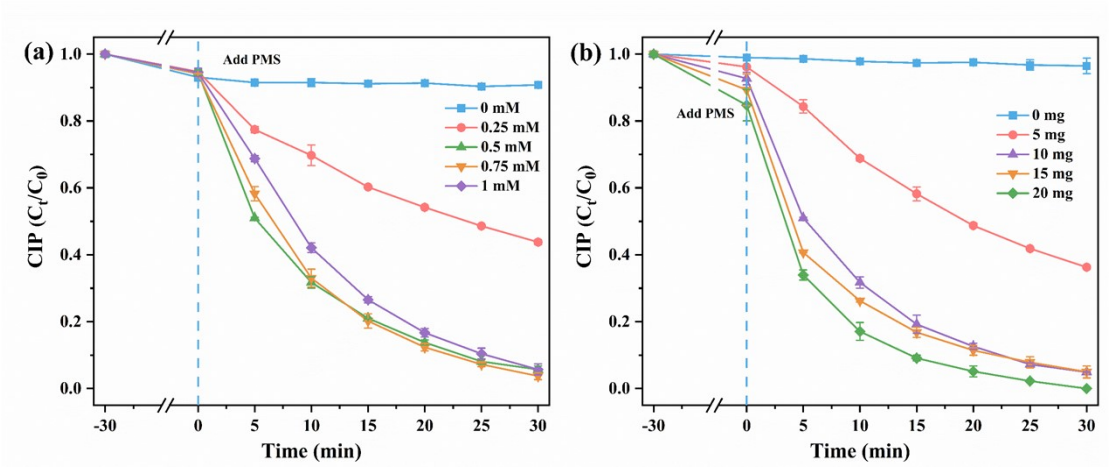

Fig. S4. Effect of PMS dosage (a) and catalyst dosage (b) on 10-CFS/PMS system.

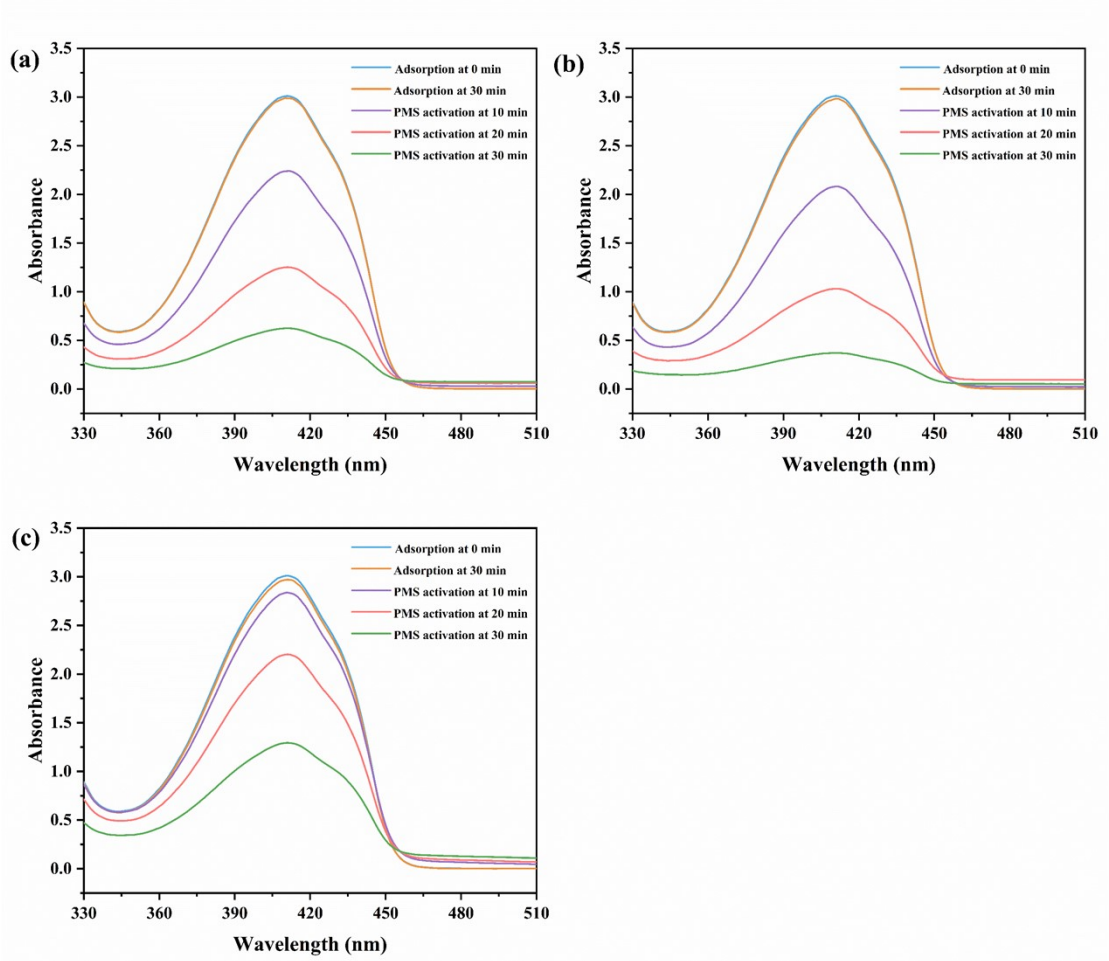

Fig. S5. Time-dependent UV-vis absorption spectrum changes of DPBF consumption in the physical mixed 10-CFS/PMS (a) 10-CFS/PMS (b) activation systems, and 10-CFS/PMS activation system with the addition of TEMPO before PMS activation (c). Reaction conditions: [CIP] = 10 mg/L, [10-CFS] = 0.1 g/L, [PMS] = 0.5 mM, [DPBF] =0.15 mM.

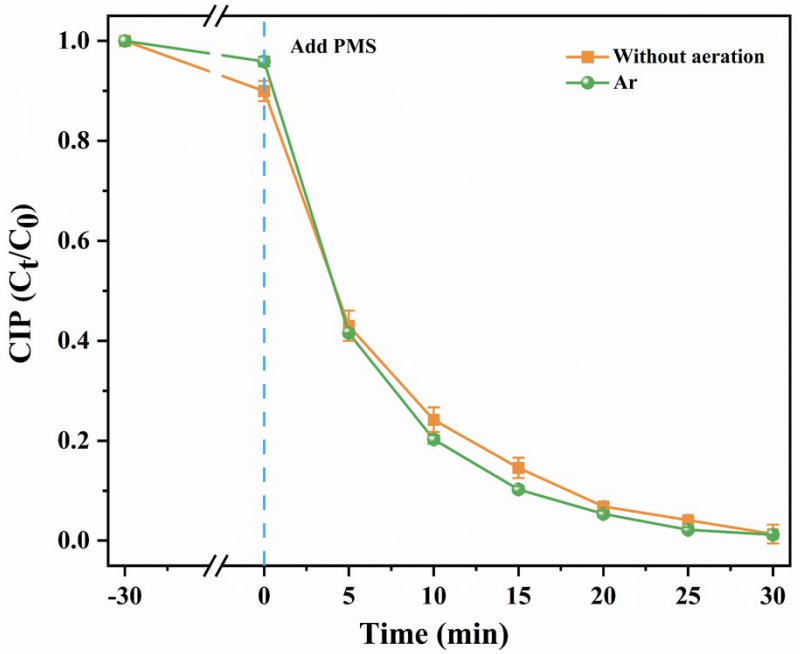

Fig. S6. CIP degradation in the 10-CFS/PMS system with or without Ar bubbling. Reaction conditions: [CIP] = 10 mg/L, [10-CFS] =0.1 g/L, [PMS] = 0.5 mM.

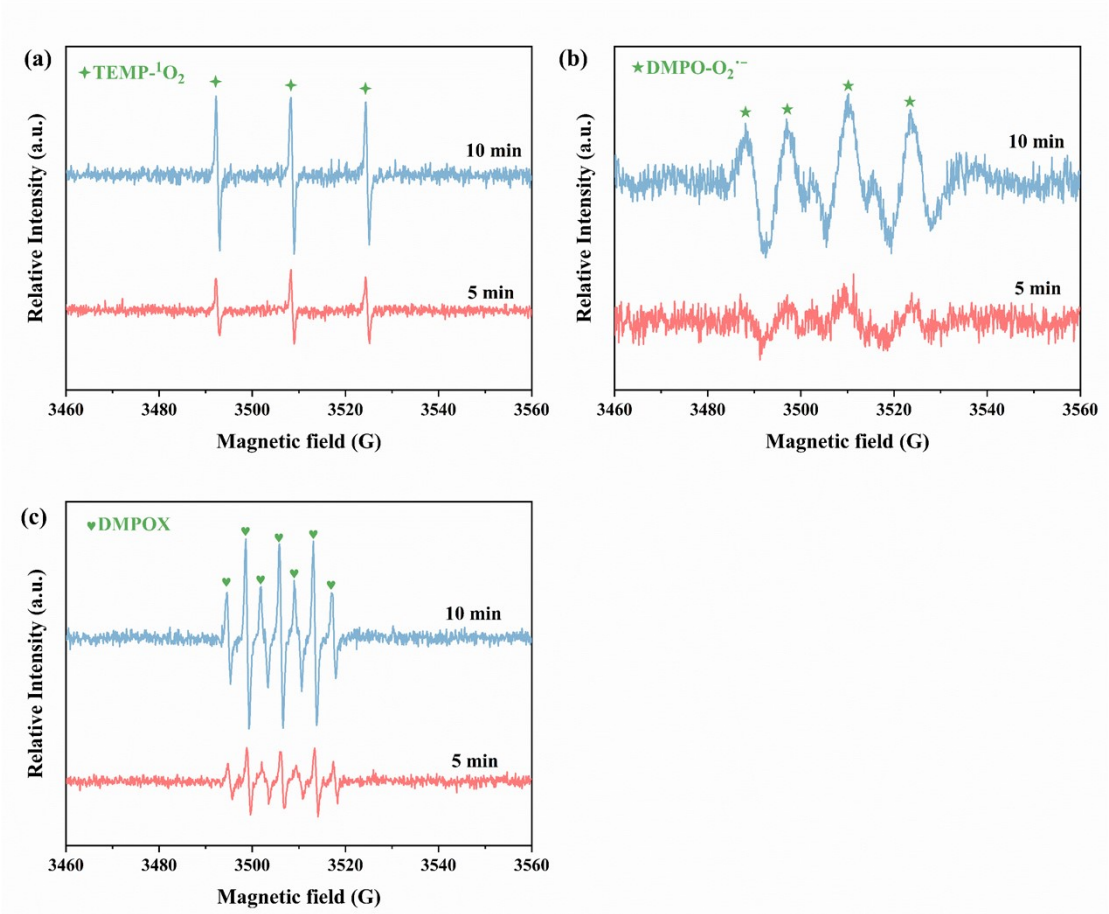

Fig. S7. EPR spectra for $^1O_2$ (a), $O_2^{\cdot-}$ (b), and $SO_4^{\cdot-}$and $HO^{\cdot}$ (c) in the 10-CFS/PMS system.

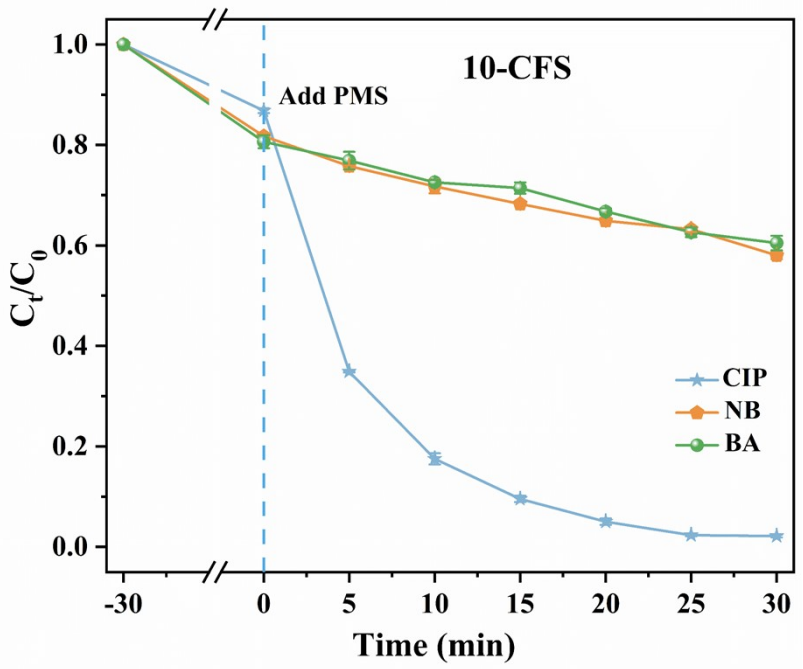

Fig. S8. Degradation efficiency of CIP, NB, and BA in the 10-CFS/PMS system. Reaction conditions: [CIP] = 10 mg/L, [NB/BA] =0.008 mM, [10-CFS] = 0.1 g/L, [PMS] = 0.5 mM.

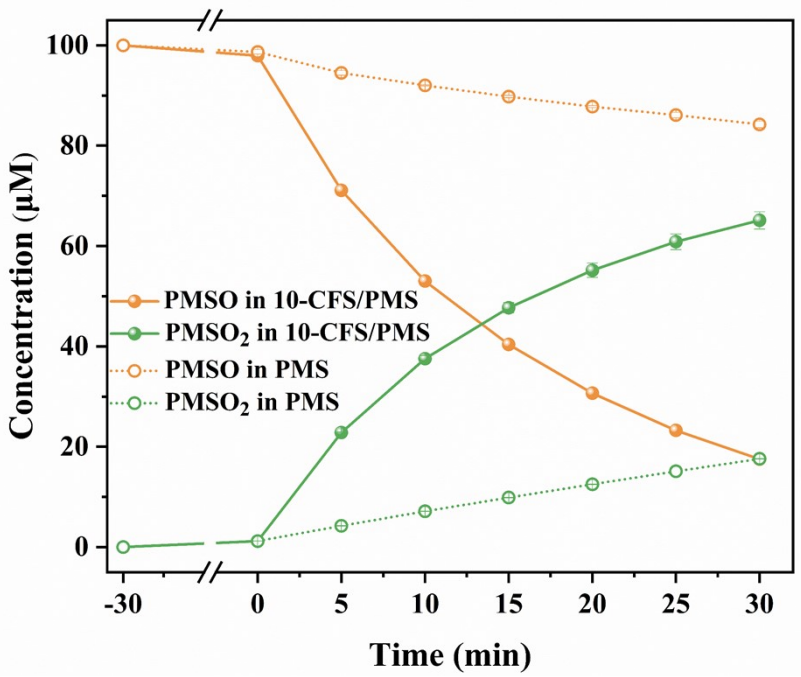

Fig. S9. Concentration variation of PMSO and $PMSO_2$ in the 10-CFS/PMS system. Reaction conditions: [PMSO]=0.1 mM, [10-CFS] = 0.1 g/L, [PMS] = 0.5 mM.

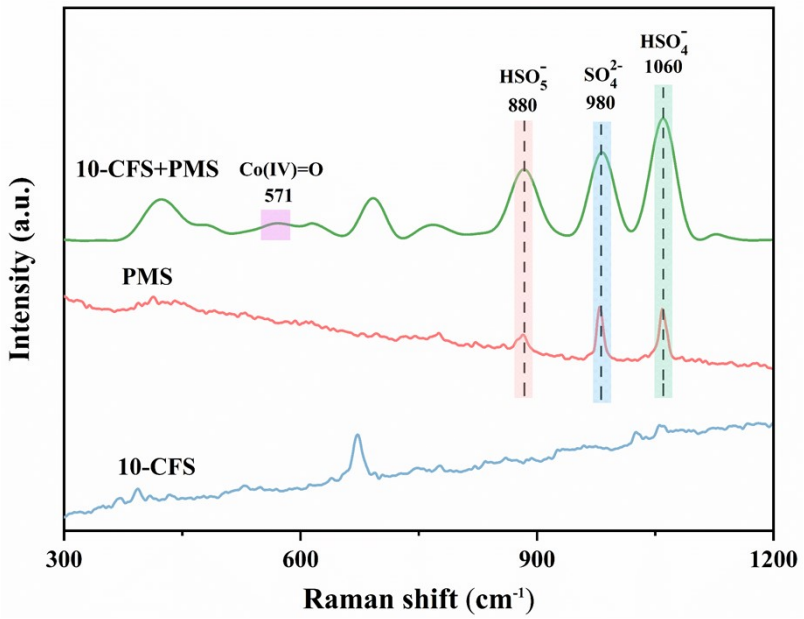

Fig. S10. In situ Raman spectra of 10-CFS/PMS system in H_2O matrix.

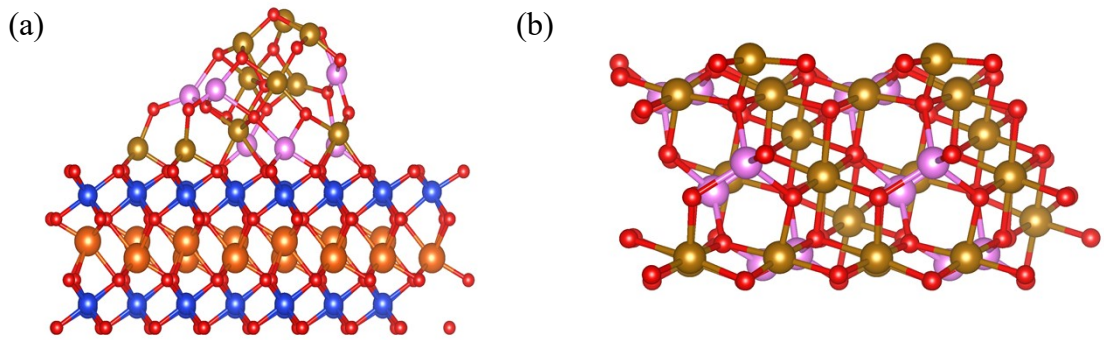

Fig. S11. The model of 10-CFS (a) and $CoFe_2O_4$ (b). The O, Mg, Si, Co and Fe atoms are represented by red, orange, blue, pink and brown spheres, respectively.

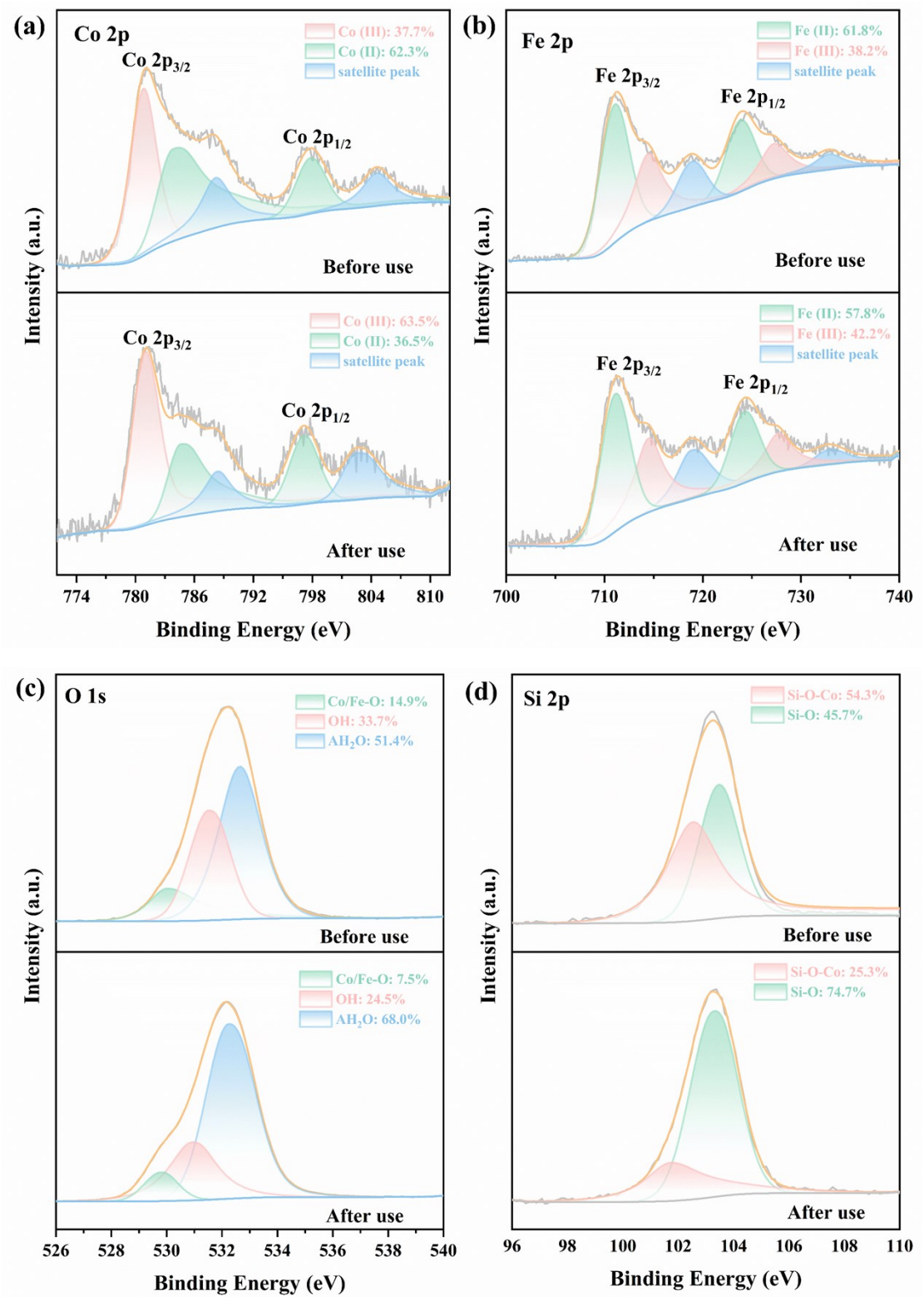

Fig. S12. XPS spectra of Co 2p (a), Fe 2p (b), O 1s (c) and Si 2p (d) of 10-CFS before and after the reaction.

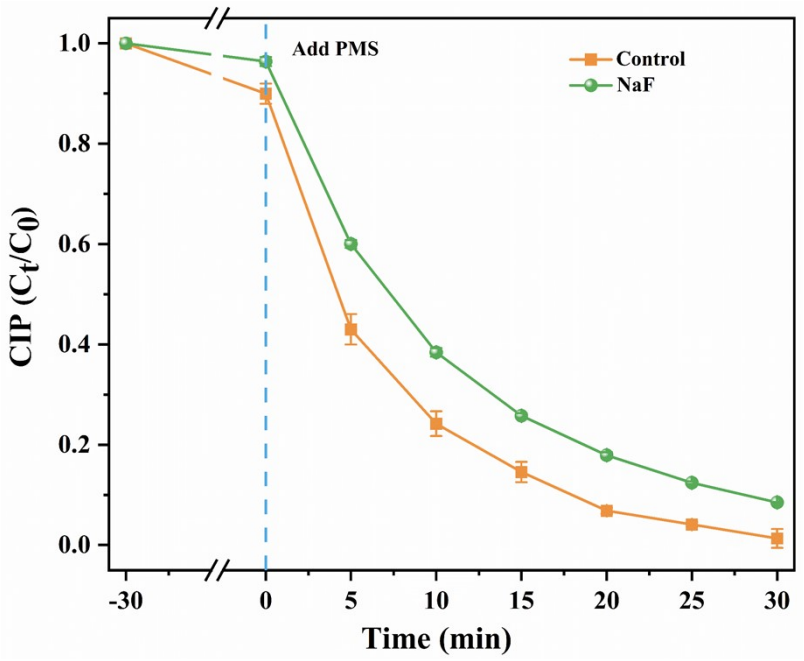

Fig. S13. The quenching experiments to prove Co and Fe active sites. Reaction conditions: [CIP] = 10 mg/L, [10-CFS] = 0.1 g/L, [PMS] = 0.5 mM, [NaF] = 2 mM.

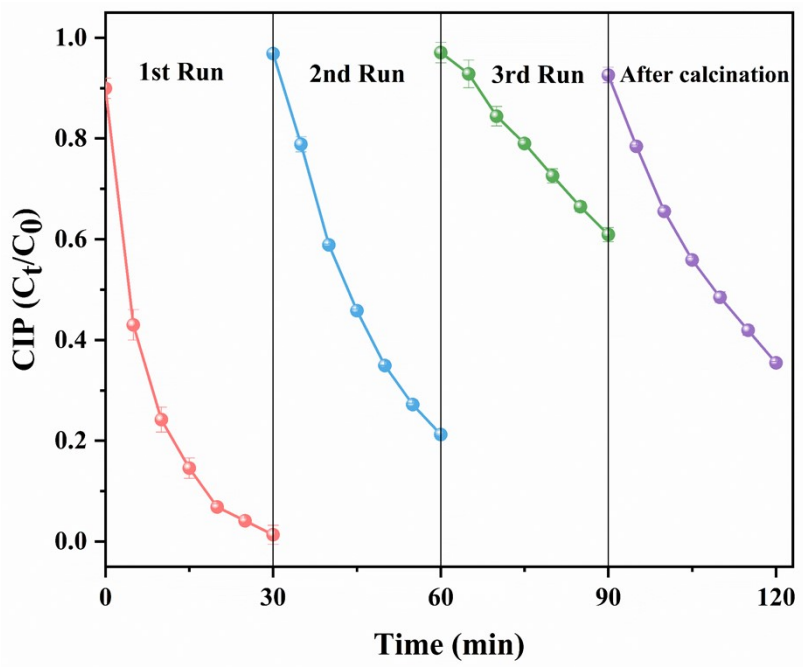

Fig. S14. Reusability of 10-CFS. Reaction conditions: [CIP] = 10 mg/L, [10-CFS] = 0.1 g/L, [PMS] = 0.5 mM.

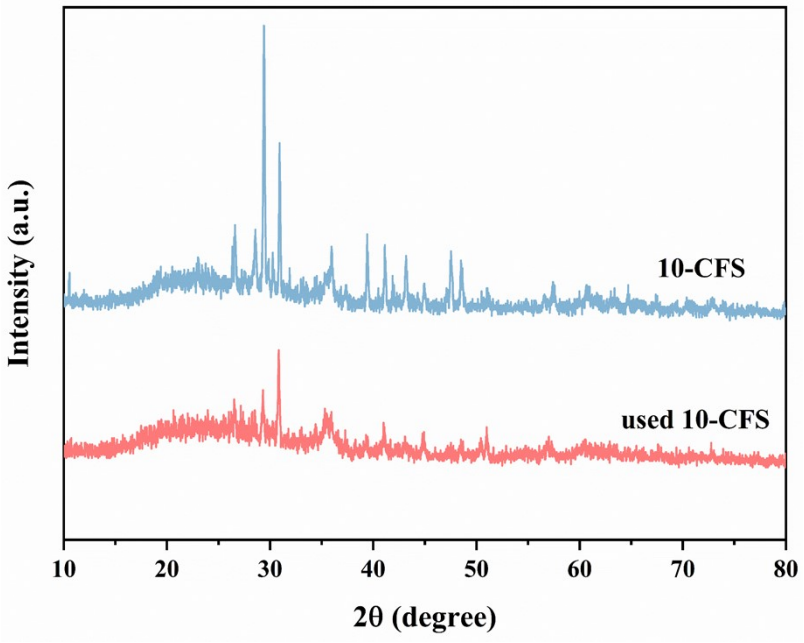

Fig. S15. XRD of fresh and used 10-CFS.

Reference

1 J. Hafner, Ab-initio simulations of materials using VASP: Density-functional theory and beyond, *J. Comput. Chem.*, 2008, **29**, 2044-2078.

2 J.P. Perdew, K. Burke and Y. Wang, Generalized gradient approximation for the exchange-correlation hole of a many-electron system, *Phys. Rev. B.*, 1996, **54**, 16533.

3 V. Wang, N. Xu, J.-C. Liu, G. Tang and W.-T. Geng, VASPKIT: A user-friendly interface facilitating high-throughput computing and analysis using VASP code, Comput. *Phys. Commun.*, 2021, **267**, 108033.

4 K. Momma and F. Izumi, VESTA: a three-dimensional visualization system for electronic and structural analysis, *J. Appl. Cryst.*, 2008, **41**, 653-658.

5 S. Grimme, J. Antony, S. Ehrlich and H. Krieg, A consistent and accurate ab initio parametrization of density functional dispersion correction (DFT-D) for the 94 elements H-Pu, *J. Chem. Phys.*, 2010, **132**, 154104.

6 A. Jain, S.P. Ong, G. Hautier, W. Chen, W.D. Richards, S. Dacek, S. Cholia, D. Gunter, D. Skinner and G. Ceder, Commentary: The Materials Project: A materials genome approach to accelerating materials innovation, *APL Mater.*, 2013, **1**, 011002.

7 J. Liang, X. Duan, X. Xu, K. Chen, Y. Zhang, L. Zhao, H. Qiu, S. Wang and X. Cao, Persulfate Oxidation of Sulfamethoxazole by Magnetic Iron-Char Composites via Nonradical Pathways: Fe(IV) Versus Surface-Mediated Electron Transfer, *Environ. Sci. Technol.*, 2021, **55**, 10077-10086.

8 Y. You, Z. Zhao, Y. Song, J. Li, J. Li and X. Cheng, Synthesis of magnetized nitrogen-doped biochar and its high efficiency for elimination of ciprofloxacin

hydrochloride by activation of peroxymonosulfate, *Sep. Purif. Technol.*, 2021, **258**, 117977.

9 B. Liu, W. Song, H. Wu, Y. Xu, Y. Sun, Y. Yu, H. Zheng and S. Wan, Enhanced oxidative degradation of norfloxacin using peroxymonosulfate activated by oily sludge carbon-based nanoparticles $CoFe_2O_4$/OSC, *Chem. Eng. J.*, 2020, **400**, 125947.

10 A. Hassani, P. Eghbali, B. Kakavandi, K.-Y.A. Lin and F. Ghanbari, Acetaminophen removal from aqueous solutions through peroxymonosulfate activation by $CoFe_2O_4$/mpg-C_3N_4 nanocomposite: Insight into the performance and degradation kinetics, *Environ. Technol. Inno.*, 2020, **20**, 101127.

11 Q. Wang, Y. Shao, N. Gao, W. Chu, J. Chen, X. Lu, Y. Zhu and N. An, Activation of peroxymonosulfate by Al_2O_3-based $CoFe_2O_4$ for the degradation of sulfachloropyridazine sodium: Kinetics and mechanism, *Sep. Purif. Technol.*, 2017, **189**, 176-185.

12 Y. You, Z. Shi, Y. Li, Z. Zhao, B. He and X. Cheng, Magnetic cobalt ferrite biochar composite as peroxymonosulfate activator for removal of lomefloxacin hydrochloride, *Sep. Purif. Technol.*, 2021, **272**, 118889.

13 N.S. Shah, J.A. Khan, M. Sayed, Z.U.H. Khan, H.S. Ali, B. Murtaza, H.M. Khan, M. Imran and N. Muhammad, Hydroxyl and sulfate radical mediated degradation of ciprofloxacin using nano zerovalent manganese catalyzed $S_2O_8^{2-}$, *Chem. Eng. J.*, 2019, **356**, 199-209.